^{1}H Solid-State NMR Investigation of Structure and Dynamics of Anhydrous Proton Conducting Triazole-Functionalized Siloxane Polymers

Ümit Akbey,[†] Sergio Granados-Focil,[‡] E. Bryan Coughlin,[§] Robert Graf,[†] and Hans Wolfgang Spiess*,[†]

Max Planck Institute for Polymer Research, Ackermannweg 10, D-55128 Mainz, Germany, Carlson School of Chemistry, Clark University, 950 Main Street, Worcester, Massachusetts 01601, and Department of Polymer Science and Engineering, University of Massachusetts, Amherst, Massachusetts 01003

Received: April 3, 2009; Revised Manuscript Received: May 26, 2009

^{1}H MAS solid-state NMR methods are applied to elucidate the conduction mechanism of an anhydrous proton conducting triazole-functionalized polysiloxane. At temperatures below $T = 260$ K, hydrogen bonding between neighboring heterocycles is observed and a dimer formation can be excluded. From the temperature dependence of ^{1}H MAS NMR spectra, different dynamic processes of the triazole ring contributing to the proton conduction process are qualitatively and quantitatively analyzed and detailed insight into the conduction mechanism and temperature-dependent structural changes is obtained. Although the dynamics processes on the molecular level are qualitatively in good agreement with the findings from macroscopic conductivity measurements, temperature-dependent factors on mesoscopic scales beyond the local molecular mobility influence the macroscopic conductivity and hamper quantitative interpretation.

1. Introduction

Fuel cells are one of the most attractive approaches to mobile, renewable alternative energy sources, due to their high flexibility and their easy handling. One of the most crucial components of such devices is the proton exchange membrane. Currently, the most commonly applied polymer membranes are based on the perfluorinated polymer Nafion. In the fully hydrated form, these membranes provide excellent proton conductivity of about 0.19 S cm^{-1} at temperatures below 100 °C,[1] which allows for high power densities and efficiencies in fuel cell applications. For technical reasons such as methanol crossover and CO poisoning of the electrodes, a high-temperature operation ($T >$ 100 °C) of fuel cells would be favorable. However, proton conduction drops dramatically in Nafion and related membranes when the proton-carrying liquid water evaporates from the membrane.

In order to avoid demanding water management systems for fuel cell applications at temperatures above 120 °C,[1,2] a new class of proton transport membranes is needed, which do not rely on the diffusion of small proton-carrying molecules (vehicular mechanism) and are independent of the overall degree of hydration of the membrane. To meet this challenging goal, several design concepts have been explored for anhydrous proton conducting polymer electrolyte membranes with moderate to fair conductivity at temperatures higher than 100 °C.

Hydrogen bonding is one of the key interactions in many chemical and biological systems, and many important phenomena rely on these interactions.[3] The motivating factor behind many of these studies is the structure-stabilizing or even structure-directing role of hydrogen bonds, which is as yet not fully understood, and represents one of the current frontiers of scientific research.[4] Solid-state NMR has been used widely to elucidate structure and dynamics of hydrogen bonded systems.[5,6] In particular, ^{1}H magic angle spinning (MAS) NMR spectroscopy is capable of distinguishing hydrogen bonds between different proton donor and acceptor groups such as O−H···O, O−H···N, N−H···O, and N−H···N and thus can provide valuable information on hydrogen bonded networks in proton conducting polymer systems.

^{1}H solid-state MAS NMR studies have been previously performed on many different types of proton conducting systems.[7−14] The first of those has been performed on imidazole-based materials, and it was found that only the weakly hydrogen bonded sites in disordered areas contribute to proton conductivity.[7] Strongly hydrogen bonded protons in many proton conducting materials show only restricted local reorientations.[8,9] The differences between macroscopic proton conductivity and local mobility was confirmed by MAS NMR studies on H_3PO_4-doped poly(benzimidazole) materials.[10] The mobility of P−OH groups, their cross-linking tendencies, and the role of disorder were studied by high-resolution solid-state MAS NMR.[8,11] Finally, proton conducting acid−base polymer blends were also investigated in detail in our group by NMR methods.[12] It was found that different types of strong hydrogen bonded protons exist at the same time in the blends and complexation supplied additional stability to the system.

The system studied here is a triazole-functionalized polysiloxane which is a promising alternative heterocyclic whose structure is similar to imidazole but contains three nitrogen atoms in the ring (structure is shown in Figure 1a). Recently, triazole was used as a protogenic solvent in a blend with acidic polyelectrolytes to generate high-temperature resistive and electrochemically stable free-standing films.[15] Polymer electrolyte membranes consisting of an acidic polymer host and triazole allowed for long-range proton transport via structural diffusion as reported before.[11,14−17]

* Corresponding author. Fax: +49-6131-379100. E-mail: spiess@mpip-mainz.mpg.de.
[†] Max Planck Institute for Polymer Research.
[‡] Clark University.
[§] University of Massachusetts.

10.1021/jp9030909 CCC: $40.75
Published on Web 06/17/2009

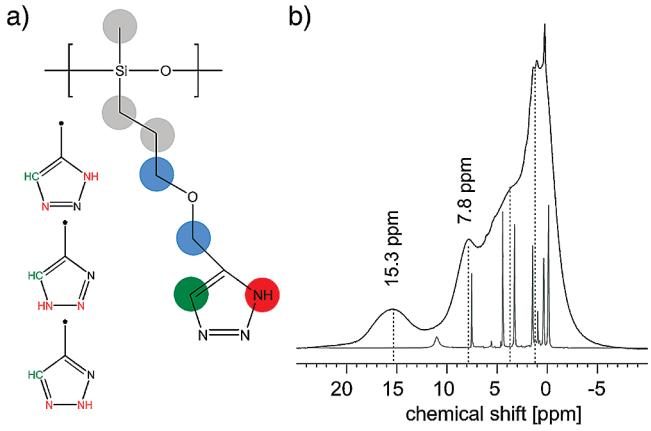

Figure 1. (a) Chemical structure of the Tz5Si material studied and its three different tautomers with different protonated nitrogen sites. (b) ^{1}H MAS NMR spectrum of Tz5Si recorded at 233 K (T_g − 47 K) and 25 kHz magic angle spinning frequency. For comparison, the spectrum of the same sample recorded at 373 K (sharp lines) is also shown.

SCHEME 1: Synthesis of Tz5Si[a]

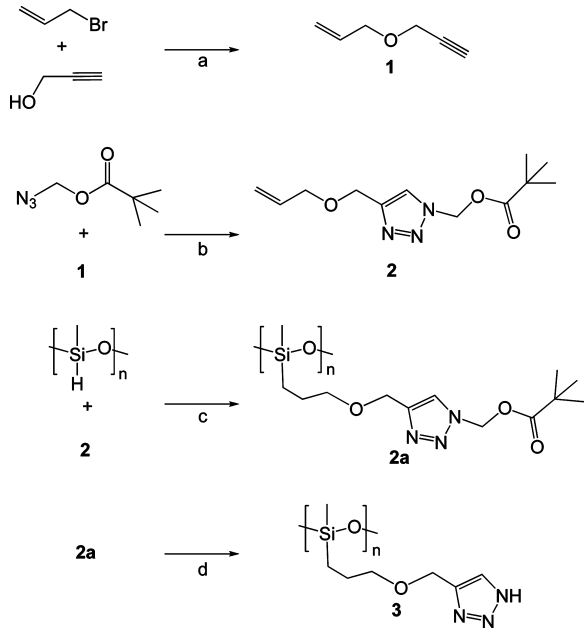

[a] (a) NaH (2 equiv), DMF, room temperature (RT), 12 h. (b) $CuSO_4$, *t*-BuOH/H_2O (1:1), sodium ascorbate, RT, 18 h. (c) Pt(0) (Karsted's catalyst), toluene, 50 °C, 36 h. (d) 0.01 M NaOH/MeOH, ethylenediamine (7 equiv), RT, 1.5 h.

2. Experimental Section

2.1. Materials. Azidomethyl pivalate was prepared as reported in the literature.[18] All other reagents were purchased from Sigma-Aldrich and used as received. Tetrahydrofuran (THF) and toluene were distilled over sodium/benzophenone prior to use. Dimethylformamide (DMF) was distilled over calcium hydride prior to use.

The triazole-functionalized polysiloxane, Tz5Si, was synthesized according to previously reported methods as illustrated in Scheme 1.[16]

2.2. Synthesis of 3-Allyloxyprop-1-yne (1). To a clean, dry, nitrogen-purged 250 mL two-neck round-bottom flask was added sodium hydride (1.44 g, 0.06 mol) and anhydrous DMF (45 mL). The slurry was cooled to 0 °C followed by dropwise addition of 3-propyn-1-ol (1.75 mL, 0.03 mol) under constant agitation. The mixture was stirred for 30 min and allowed to come to room temperature. Allyl bromide (2.46 mL, 0.028 mol) was added dropwise under constant agitation, and the mixture was allowed to stir for 2 h at room temperature. The reaction was ended by addition of a large excess of water (200 mL), and the product was extracted with dichloromethane (5 × 25 mL). The combined organic layers were dried over anhydrous $MgSO_4$ and filtered through a silica pad; solvent was removed under reduced pressure to yield 3-allyloxy-prop-1-yne (**1**) as a pale yellow liquid (1.94 g, 72%) which was used without further purification. ^{1}H NMR ($CDCl_3$) δ 1.95 (1H, t), 2.22 (2H, m), 3.47 (2H, m), 3.96 (2H, d), 5.18 (1H, dd), 5.25 (1H, dd), 5.89 (1H, m). ^{13}C NMR ($CDCl_3$) δ 68.42, 69.71, 71.81, 84.33, 116.78, 134.96.

2.3. Synthesis of 4-(Allyloxymethyl)-[1,2,3]triazol-1-ylmethyl Pivalate (2). To 1.5 g (15.6 mmol) of **1**, were added a mixture of *t*-BuOH/water (2/1) (93 mL) and $CuSO_4 \cdot 5H_2O$ (1.5 mL of a 1.0 M solution, 1.5 mmol) followed by a 1.0 M solution of sodium ascorbate (3.0 mL, 3.0 mmol) and azidomethyl pivalate (2.83 g, 18 mmol). The mixture was stirred vigorously for 18 h at room temperature. The reaction was diluted with water, and the product was extracted with ethyl acetate (2 × 100 mL). The combined organic layers were washed with 5% NH_4OH (2 × 100 mL) and brine, dried over $MgSO_4$, and filtered; solvent was removed under reduced pressure. Purification was performed by flash chromatography (ethyl acetate/hexanes 1:1) to yield 4-(allyloxymethyl)-[1,2,3]triazol-1-ylmethyl pivalate (3.51 g, 89%). ^{1}H NMR ($CDCl_3$) δ 1.18 (9H, s), 4.08 (2H, t), 4.64 (2H, d), 5.14 (1H, d), 5.23 (1H, d), 5.89 (1H, m), 6.21 (2H, s), 7.79 (1H, s). ^{13}C NMR ($CDCl_3$) δ 25.06, 39.34, 69.39, 69.67, 71.57, 116.57, 121.91, 134.68, 148.39, 177.56.

2.4. Synthesis of Tz5Si (3). In a drybox, 1.26 g (5 mmol) of **2**, 200 mg (3.3 mmol) of polymethylhydrosiloxane (PHMS) and 5 mL of dry toluene were added to a glass vial equipped with a magnetic stirrer and a rubber septum. The mixture was stirred for 5 min and then 5 drops of Karstedt's catalyst (0.1 M solution in polydimethylsiloxane) were added; the solution changed from colorless to light yellow. After addition of the catalyst the vial was removed from the drybox and stirred at 75 °C for 48 h. The reaction was then diluted with diethyl ether (10 mL) and filtered through a silica pad followed by extensive washing with ether (100 mL). The excess solvent was removed by rotary evaporation, and purification was accomplished by column chromatography. A mixture of ethyl acetate:hexanes (1:1) was used to remove the unreacted allyloxymethyltriazole (**2**); the pivaloyloxymethyl protected triazole (POM) functionalized siloxane (POM-Tz5Si) polymer was removed from the column by elution with ethyl acetate:methanol 5:1. The pivaloyl protecting group was removed by treatment with sodium methoxide. To a clean, dry, 100 mL round-bottom flask equipped with a stir bar was added triazole-POM functionalized polysiloxane (500 mg, 1.6 mequiv) and ethylenediamine (235 μL, 7.05 mequiv). Under constant agitation, 0.1 M NaOH/MeOH (31 mL, 3.1 equiv) was added to the flask. The reaction mixture was stirred for 90 min, and then poured slowly into pH 7 buffer solution. The buffer pH was monitored and kept from exceeding pH 8 by adding 1.0 M HCl as necessary. Final pH was adjusted to 8 followed by extraction with ethyl acetate:dichloromethane (1:1) (5 × 30 mL) to remove the polymer (triazole-5-siloxane, Tz5Si, **3**). Solvent was removed under reduced pressure to yield an opaque viscous oil (256 mg, 82%). ^{1}H NMR (DMSO-d_6) δ 0.042 (3H, s), 0.48 (2H, m), 1.70 (2H, quin), 3.69 (4H, bs), 7.84 (1H, s), 14.3 (1H, s). ^{13}C NMR (DMSO-d_6) δ −0.81, 12.45, 24.30, 69.58, 71.54, 131.58, 146.28.

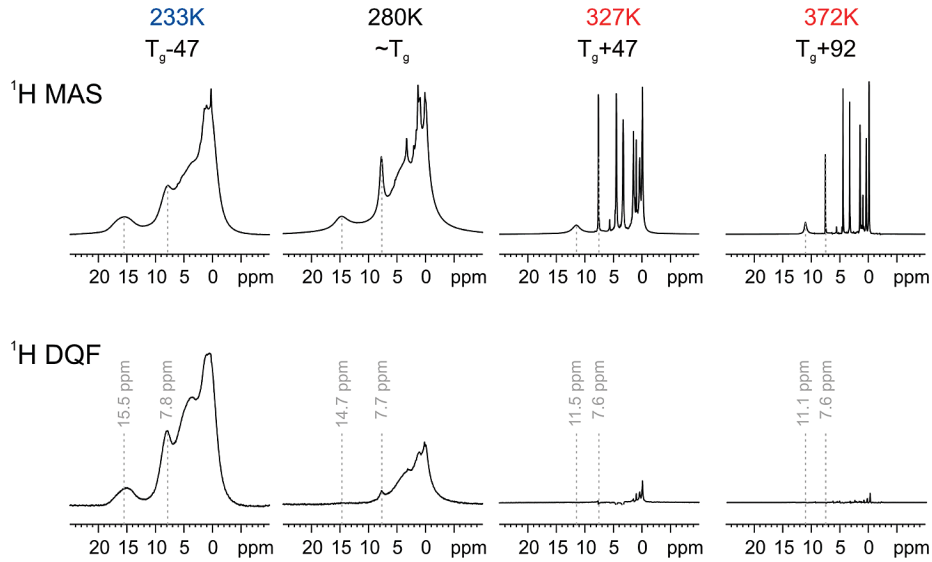

Figure 2. ^{1}H MAS and DQF spectra of Tz5Si at various temperatures (233, 280, 327, and 372 K) recorded at 25 kHz MAS spinning frequency. The back-to-back pulse sequence was applied during one rotor period (40 μs) for DQ excitation and reconversion to obtain the double-quantum-filtered spectra.

Thermogravimetric analysis (TGA) was carried out using a TA Instruments TGA 2950 thermogravimetric analyzer with a heating rate of 10 °C/min from room temperature to 600 °C under nitrogen purge. Glass transition temperatures were obtained by differential scanning calorimetry (DSC) using a TA Instruments Dupont DSC 2910. Samples, approximately 3−5 mg, were used with a heating rate of 10 °C/min from −100 to 180 °C under a flow of nitrogen (50 mL/min); the midpoint of the observed step transition was taken as T_g.

^{1}H and ^{2}H MAS NMR experiments were performed on a Bruker Avance spectrometer operating at ^{1}H and ^{2}H Larmor frequencies of 700.13 and 107.46 MHz, respectively, using a commercial double resonance probe with 2.5 mm MAS rotors spinning up to 30 kHz. All temperatures reported here have been corrected for frictional heating caused by high MAS frequencies (>20 kHz) according to the procedure proposed by Bielecki et al.[19] Double-quantum (DQ) coherences used for DQ filtration or for single-quantum (SQ)−DQ correlation under fast MAS conditions were excited using the back-to-back (BABA) recoupling pulse sequence.[20] Phase-sensitive two-dimensional DQ experiments have been recorded with 64 rotor synchronized t1 increments using the States-TPPI method.[21]

^{13}C cross-polarization (CP) MAS NMR spectra were recorded on a Bruker DSX spectrometer at 125.47 MHz ^{13}C Larmor frequency. All CP-MAS spectra have been recorded with 1 ms contact time, 100 kHz rf nutation frequency for both proton and carbon (2.5 μs 90° pulse length), at 15 kHz MAS frequency, and by using the TPPM scheme for proton decoupling.[22]

3. Results and Discussion

Thermogravimetric analysis of Tz5Si showed that the polysiloxane remains thermally stable up to 180 °C under nitrogen. Slow heating (1 °C/min) under air produced a 10% weight loss at 175 °C, suggesting that the chemical structure would require further optimization before being used for membrane electrode assemblies. However, the materials are stable to the conditions used during impedance and NMR measurements. Moreover, thermal cycling of the polymer samples under vacuum did not produce appreciable changes in the electrical impedance or the chemical structure. The glass transition temperature of the 1,2,3-triazole containing polysiloxane as determined by DSC was 5 °C, which is consistent with the trend observed for other previously reported polysiloxanes.[16]

^{1}H MAS NMR spectra will supply chemical shift information of different proton sites. This information gives a first idea on local packing arrangements since the proton chemical shift is sensitive to supramolecular noncovalent interactions such as ring current effects due to $\pi-\pi$ packing of aromatic moieties or hydrogen bonding,[5] which is the dominating interaction in the system studied here. In addition to this information, ^{1}H variable-temperature (VT) MAS NMR will elucidate the local proton mobility and time scales of molecular motions, which can be compared to proton conductivity. Comparing ^{1}H MAS spectra to the ^{1}H double-quantum-filtered (DQF) MAS spectra will allow us to distinguish mobile and rigid proton sites. Moreover, spatial proximities between proton sites will be obtained in a semiquantitative manner by the use of two-dimensional (2D) ^{1}H DQ MAS NMR. By chemical exchange with perdeuterated solvents, selective deuteration of the acidic NH protons at the triazole ring can be achieved, and local dynamic processes of the amine site can be studied selectively using ^{2}H NMR methods.

3.1. One-Dimensional ^{1}H MAS and DQF MAS NMR: Structure of the System. Basic information on the local organization of the system can be obtained from simple ^{1}H MAS NMR experiments, since the proton chemical shift is sensitive to noncovalent supramolecular interactions such as the spatial proximity of aromatic moieties via the ring current effect or, more relevant for the current system, hydrogen bonding. The ^{1}H MAS NMR signals of the hydrogen bonding sites are shifted to lower fields, thus to higher parts per million (ppm) values,[5] and the magnitude of this low-field shift correlates with the strength of the hydrogen bond as well as the type of donor and acceptor molecules. There are well-established correlations between the distance of the two electronegative atoms (O···O, O···N, or N···N) involved in hydrogen bonding and the observed proton chemical shift.[23−25] This type of correlation for the N−H···N case is particularly important to estimate the structure of the hydrogen bonded network in the current system.[26−28] Chemical shift values between 14 and 18 ppm have been reported previously for hydrogen bonded NH protons.[11,12]

Figure 2 shows the ^{1}H MAS spectrum of Tz5Si recorded at $T = 233$ K (~50 K below the glass transition temperature T_g) and 30 kHz MAS. Due to the low molecular mobility at this temperature, the proton resonances are quite broad and only four different signals can be distinguished: the aliphatic region (H_a) with some fine structure at 1−2 ppm, OCH_2 (H_b) signals around 4 ppm, aromatic proton signals (H_c) at 8 ppm, and the hydrogen bonding NH (H_d) protons around 15.5 ppm. The high chemical shift value of 15.5 ppm of the triazole NH proton signal indicates that this proton site is involved in a strong hydrogen bond. From quantum chemical studies correlating distances of hydrogen bonded atoms and their chemical shifts in an imidazole-based material with typical N−H···N type hydrogen bonds,[28] a distance of ~2.8 Å between the two N atoms involved in the hydrogen bond can be estimated. The spectral resolution of aromatic CH and NH protons will allow us to study the local dynamics of the aromatic triazole ring and hydrogen bonding separately; vide infra.

^{1}H MAS NMR methods are very sensitive probes for local molecular dynamics, since molecular mobility averages the orientation-dependent NMR interactions such as dipolar couplings as well as heterogeneous distributions of chemical shifts resulting from different local packing arrangements in disordered solids.[29] Both phenomena will cause a reduction of the line width with increasing temperature and thus increasing molecular mobility. Another sensitive probe for molecular mobility are double-quantum-filtered (DQF) ^{1}H MAS NMR spectra, where local dipolar couplings are used to excite double-quantum coherences, which can be selected by an appropriate phase cycling.[5,6] The signal intensity reflects the dipolar couplings to neighboring proton sites, so the proton signals should decrease rapidly at the onset of molecular motion and finally vanish when the molecular motion becomes fast and isotropic. Moreover, spatially isolated proton sites will be suppressed by double-quantum filtration independent of their dynamic behavior. Figure 2 shows ^{1}H MAS and ^{1}H DQF MAS NMR spectra recorded at various selected temperatures. At temperatures well below the glass transition temperature, $T \sim T_g - 50$ K, the ^{1}H MAS and DQF spectra are very similar. Only a minor, sharp aliphatic component at 1 ppm left from the chemical deprotection procedure is reduced by the double-quantum filtration and the O−CH_2 groups enhanced. The similarity of the two spectra indicates that the sample is rigid on a millisecond time scale at this temperature. At $T = 280$ K, close to the glass transition temperature (T_g) of the sample, the ^{1}H MAS NMR signals start to narrow. In the DQF MAS NMR spectrum the signal of the aromatic protons is strongly reduced and the signal of the hydrogen bonded NH protons is almost completely suppressed. This shows that the NH protons are already mobile on the time scale of the double-quantum filtration, which has been performed with 40 μs double-quantum excitation time corresponding to one rotor period recoupling time at 25 kHz MAS spinning frequency. The signals of proton sites of the polymer backbone, or the linker, are less affected by the double-quantum filtration. This demonstrates that the molecular motion starts at the end of the side chains. At temperatures well above T_g, all resonances in ^{1}H MAS are narrowed due to increasing molecular mobility. As a result of the higher local mobility, the dipolar couplings of the proton sites are reduced. This leads to a substantial signal decrease in the DQF spectra, where, at the highest temperature, only aliphatic proton sites of the polymer backbone are observed. First, we will discuss the dynamic behavior of the sample causing the obvious line narrowing effects and chemical shift changes observed in the temperature dependence of the ^{1}H MAS spectrum. As a starting point, the local packing arrangement of the sample as it is seen by two-dimensional double-quantum NMR spectroscopy under MAS (DQ MAS NMR) will be examined.

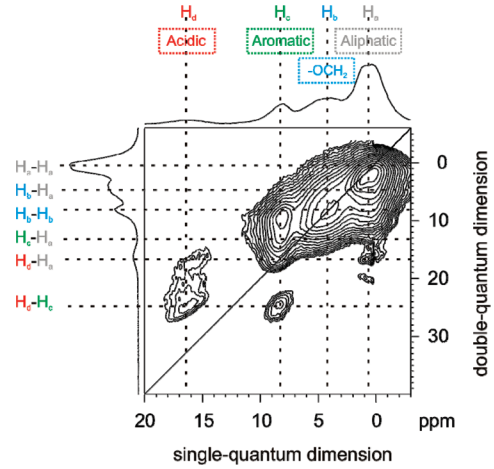

Figure 3. Two-dimensional ^{1}H DQ MAS NMR spectra of Tz5Si recorded at 233 K and 25 kHz MAS using one rotor period of back-to-back DQ recoupling for double-quantum excitation and reconversion.

3.2. Two-Dimensional Rotor-Synchronized ^{1}H DQ MAS NMR: Proton Proximities and Order in the System in the Solid Phase. Semiquantitative information on spatial proximities between the spectrally resolved proton sites can be obtained by a two-dimensional ^{1}H DQ MAS spectrum, recorded with rotor-synchronized time increments for the DQ dimension, a short DQ excitation time of only one rotor period BaBa DQ recoupling under fast MAS conditions ($\upsilon_{MAS} = 25$ kHz). Since we now focus on local packing arrangements, this DQ MAS NMR spectrum was taken at low temperature ($T = 233$ K $\sim T_g - 50$ K), where molecular mobility is almost completely frozen on the time scale of the DQ experiment (two MAS rotor periods) and thus the DQ excitation efficiency is determined by static dipolar couplings depending on the inverse of the internuclear distance cubed between the proton sites. The experimental result for our sample is given in Figure 3. As suggested by the chemical structure of the material, strong DQ signals between spins with like chemical shifts, so-called autopeaks, are observed at 1/2 ppm and 4/8 ppm in the SQ/DQ dimension for the aliphatic and OCH_2 proton sites, respectively.[5] DQ signals between spins with different chemical shifts, so-called cross-peaks, are split into two signals, which are observed in the DQ dimension at the sum of the chemical shifts of the interacting spins and in the SQ dimension at the chemical shifts of both spins involved.

The most pronounced cross-peak in the DQ MAS NMR spectrum was observed between aromatic and aliphatic proton sites, though these two species are well separated in the chemical structure of the molecule, and a more pronounced correlation between aromatic and OCH_2 sites than would be suggested by the chemical structure. In contrast to the unexpectedly intense DQ correlation of the aromatic and aliphatic proton sites close to the polymer backbone, the DQ cross-peaks between hydrogen bonded and aliphatic proton sites at 1/17 ppm and 16/17 ppm have very low intensity and are much weaker than the correlation between hydrogen bonded and aromatic proton sites at 8.5/25 ppm and 16.5/25 ppm. The latter, however, could be expected from the chemical structure, as both the hydrogen bonded site and the aromatic proton site are located on the triazole ring and are in neighboring positions in one of the three

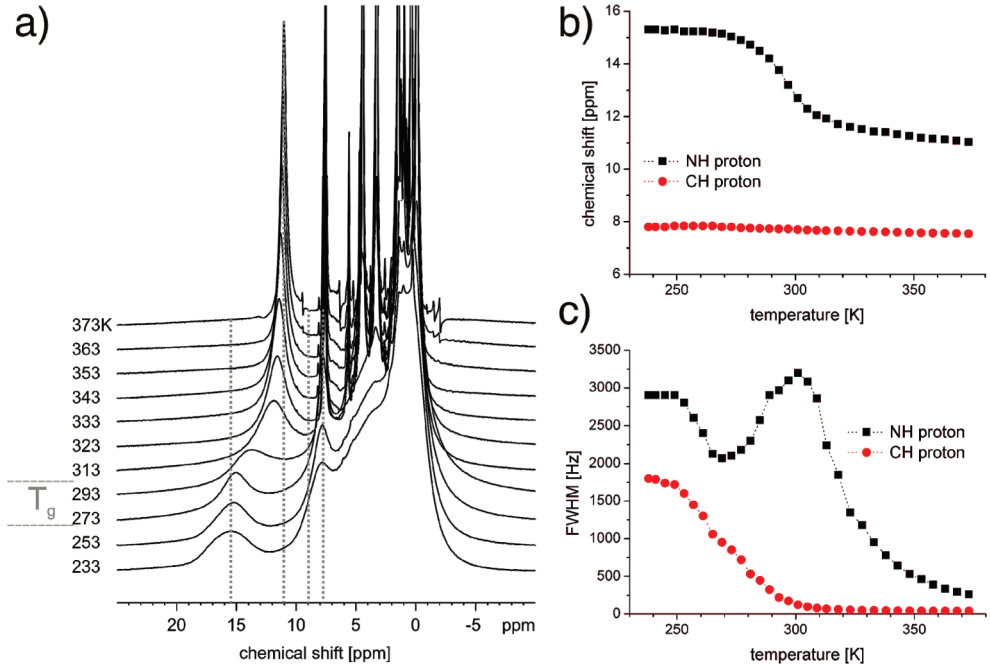

Figure 4. (a) ^{1}H variable-temperature MAS NMR spectra of Tz5Si recorded at 25 kHz MAS. Pronounced line narrowing at all proton resonances can be seen at elevated temperatures. (b) Chemical shift changes ring-CH and NH at various temperatures. (c) Full-width line widths changes ring-CH and NH at half-maximum at different temperatures.

tautomers (see Figure 1). Concerning the intensities of the cross-peaks, it should be pointed out that the expected equal intensity of the two cross-peaks is observed only if both nuclei involved show a similar relaxation behavior. This assumption, however, fails in many cases when mobile species like methyl groups or hydrogen bonding protons are involved in such double-quantum experiments. More remarkable is the autopeak of aromatic proton sites at 8.5/17 ppm, because it results from a close spatial proximity of neighboring triazole rings, since there is only a single aromatic CH site on each triazole ring. Finally, it should be pointed out that even a missing signal in such a DQ MAS NMR spectrum can provide information on the local packing arrangement. In the given case, all possible arrangements where two hydrogen bonds are connecting two neighboring triazole rings can be excluded, since such a local packing would lead to an autopeak between two hydrogen bonded protons at 15/30 ppm in the DQ spectrum, which is not observed in the experiment. The hydrogen bonded network between the triazole rings in our material is thus formed by spatially separated N−H···N hydrogen bridges in contrast to dimerlike structures, which were found in imidazole-based materials studied by Goward et al.[7]

To summarize this section, there is no clear evidence for a pronounced spatial separation of the triazole rings and the aliphatic hydrophobic polymer backbone by the linker. However, the strong DQ signal between aromatic and aliphatic proton sites, in contrast to the weak signal between hydrogen bonded and aliphatic proton sites, indicates that the more acidic hydrogen bonding site avoids the hydrophobic siloxane backbone. Moreover, the triazole rings tend to be in close spatial proximity, as indicated by the autopeak of aromatic CH proton sites.

3.3. Variable-Temperature NMR Measurements. NMR measurements performed at variable temperatures provide detailed information on local molecular mobility and dynamic processes in the sample. In most cases, local molecular dynamics leads to characteristic line-broadening and line-narrowing phenomena, and in unfavorable cases may even cause an almost complete suppression of the NMR signals. In Tz5Si, both ^{13}C CP-MAS signals and ^{1}H double-quantum filtered NMR signals vanish in a narrow temperature range from 260 to 280 K. Since both NMR methods make use of dipolar couplings to generate the signal intensity, the observed loss of signal indicates the onset of large-amplitude molecular dynamics on the kilohertz time scale, which reduces both ^{1}H−^{13}C heteronuclear dipolar couplings needed for polarization transfer in the CP-MAS experiment and ^{1}H homonuclear dipolar couplings needed for double-quantum excitation. A closer look at the temperature dependence of the ^{13}C CP-MAS and ^{1}H DQ filtered spectra shows that all signals from the triazole ring and the linker to the backbone vanish around $T = 260$ K for the ^{13}C CP-MAS experiment and around $T = 270$ K for the ^{1}H DQ filtered NMR experiment. The difference in temperature reflects the different time scales of the two experiments (in the data presented here, 1 ms for the CP-MAS experiment versus one MAS rotor period of 40 μs for the DQ filtered experiment). In both cases, the signals from the methyl group of the siloxane polymer backbone are reduced last. This demonstrates that local fluctuations of the side chains are efficient enough to reduce the magnitude of motionally averaged NMR interactions at lower temperatures, and that the molecular motion of the polymer backbone is the last dynamic process to become isotropic on the time scale of the NMR experiments ranging from microseconds to milliseconds.

Much more detailed information can be obtained by analyzing the temperature dependence of the ^{1}H MAS spectra given in Figure 4a. All ^{1}H NMR signals except that assigned to the nitrogen bound protons show a continuous line narrowing with increasing temperature. In most cases, this line narrowing coincides with a change in line shape from a broad Gaussian with a rounded top at low temperatures to a narrow Lorentzian line with a sharp top at elevated temperatures. This behavior is most clearly seen for the aromatic CH signal of the triazole ring and characteristic for a heterogeneous Gaussian distribution of randomly exchanging sites, where the exchange process is frozen at low temperatures and speeds up with increasing temperature. The temperature dependence of the ^{1}H NMR signal assigned to the NH protons, however, is much more complex.

In the temperature range 233−273 K, it shows the typical line narrowing combined with a change from a Gaussian to a Lorentzian line shape. In the range $T = 270-300$ K the line broadens with increasing temperature and the line width determined at $T = 300$ K is even larger than that determined at the lowest temperatures. At the same time, the signal shifts from ∼15 ppm at 273 K to ∼12 ppm at 303 K. As the temperature increases further, the signal narrows again and shifts slowly toward lower ppm values, reaching ∼11 ppm at $T = 373$ K. Temperature-dependent changes in chemical shift of the aromatic CH site and the NH site of the triazole ring are given in Figure 4b, and the temperature dependence of their line widths is shown in Figure 4c.

Both the temperature dependence of the line width and the chemical shift of the NH site are governed by chemical exchange processes between the NH···N hydrogen bonded and the non-hydrogen bonded states, and thus the formation and breaking of hydrogen bonds at the protonated nitrogen site. This process is essential for the anhydrous proton conduction of the sample, will therefore be analyzed in detail.

3.4. Chemical Exchange of the NH Protons at the Triazole Ring. The experimental observations for the NH signal from variable-temperature ^{1}H MAS NMR experiments are attributed to exchange processes between a NH···N hydrogen bonded state and a free NH state.

$$\mathrm{NH\cdots N} \underset{k_b}{\overset{k_f}{\rightleftharpoons}} \mathrm{NH} + \mathrm{N} \tag{1}$$

where k_f and k_b refer to the rate constants in units of s^{-1} of the forward reaction and the back reaction, respectively. If the degree of dissociation of the hydrogen bonds is described by a coefficient a, such that the number of hydrogen bonded sites is given by $1 - a$ and the number of free NH sites is given by a, the thermodynamic equilibrium constant, K, can be written as

$$K = \frac{[\mathrm{NH}][\mathrm{N}]}{[\mathrm{NH\cdots N}]} = \frac{a^2}{1-a} = \frac{k_f}{k_b} \tag{2}$$

provided that the system is at equilibrium, so that the fractions of hydrogen bonded and nonbonded sites do not change with respect to time.

The effect of a two-site chemical exchange on an NMR spectrum is well-known and depends on the relative ratio of the rate constant, k, and the frequency difference $\Delta\nu$ between the NMR resonances of the exchanging sites.[30] In the slow exchange limit, when $k \ll \Delta\nu$, both resonances can be observed at their chemical shifts, with amplitudes depending on the equilibrium population of the two sites. In the fast exchange limit, when $k \gg \Delta\nu$, a single resonance is observed at a spectral position between the resonance of the two exchanging sites, and the observed chemical shift δ_{obs} is determined by the relative population and the chemical shifts of the two exchanging sites. In our case, the δ_{obs} can be determined using the dissociation coefficient a:

$$\delta_{obs} = (1-a)\delta_{\mathrm{NH\cdots N}} + a\delta_{\mathrm{NH}} \tag{3}$$

where $\delta_{\mathrm{NH\cdots N}}$ and δ_{NH} refer to the chemical shifts of the hydrogen bonded site and the free state of the NH proton, respectively. Between these two limiting cases, in the so-called intermediate motional regime, an increasing exchange rate first leads to a broadening of the two resonances combined with a shift of the two resonances toward the weighted averaged frequency until the two resonances merge at the coalescence point. Upon further increase of the exchange rate, the single NMR signal at the weighted average frequency narrows. When the line width is reduced by more than a factor of 3 compared to that at the coalescence point, the rate constant k of the exchange process can be estimated based on the line width Δ and the frequency difference $\Delta\nu$ between the two exchanging sites.[30,31]

$$k = \frac{\pi}{2}\frac{(\Delta\nu)^2}{\Delta} \tag{4}$$

Combining eqs 2 and 3, the thermodynamic equilibrium constant of the hydrogen bonding can be determined from the chemical shift of the exchange signal, whereas the rate constants of the hydrogen bond formation and breaking of the heterocyclic NH bond can be extracted from the NMR line width according to eq 4.

Please note that the quantitative analysis of the exchange process requires in all cases the knowledge of the chemical shifts of the hydrogen bonded site and the free site. The chemical shift in the hydrogen bonded state can be determined from the NMR spectra recorded at the lowest temperatures to be $\delta_{\mathrm{NH\cdots N}} = 15.3$ ppm and, as shown in Figure 4b, is almost temperature independent in this temperature range. The chemical shift of the non-hydrogen bonded/free state, however, is not observed in this spectrum, most likely due to its low amplitude and overlap with other NMR signals. The chemical shift of the NH signal at highest temperatures does not correspond to the chemical shifts of the free amine site but is governed by the exchange process and depends on the equilibrium constant K at this temperature as indicated by the observed temperature dependence of the signal.[32] Therefore, the chemical shift of the non-hydrogen bonded amine site at the triazole ring has been estimated to be $\delta_{\mathrm{NH}} \sim 9.0$ ppm from comparable polymeric compounds with triazole side groups, where a temperature-independent NH chemical shift at highest temperatures is observed (see Supporting Information).

From the temperature dependence of the equilibrium constant K, the standard reaction enthalpy ΔH and the entropy ΔS can be determined, using the following thermodynamic relation:

$$\ln K = -\frac{\Delta H}{RT} + \frac{\Delta S}{R} \tag{5}$$

where R refers to the gas constant. The determined temperature dependence is plotted in Figure 5a and shows the presence of two different processes. The reaction enthalpy of 98 ± 3 kJ/mol and the pronounced change in entropy of 316 ± 8 kJ/mol·K of the low-temperature process are both 2−4 times higher than typical values expected for the breaking of a single hydrogen bond. Thus, the observed low-temperature process originates from a collective phenomenon involving several triazole units. In fact, the low-temperature process starts around the temperature where the static glass transition is observed by DSC, and hence can be correlated with structural changes of the triazole rings at the glass transition of the polymeric material. It should be pointed out that the observed Arrhenius behavior of the dynamics indicates a strong glass former[33] and that the estimated collectivity is relatively low for a structural transition. This indicates that the hydrogen bonding rather than the dynamics

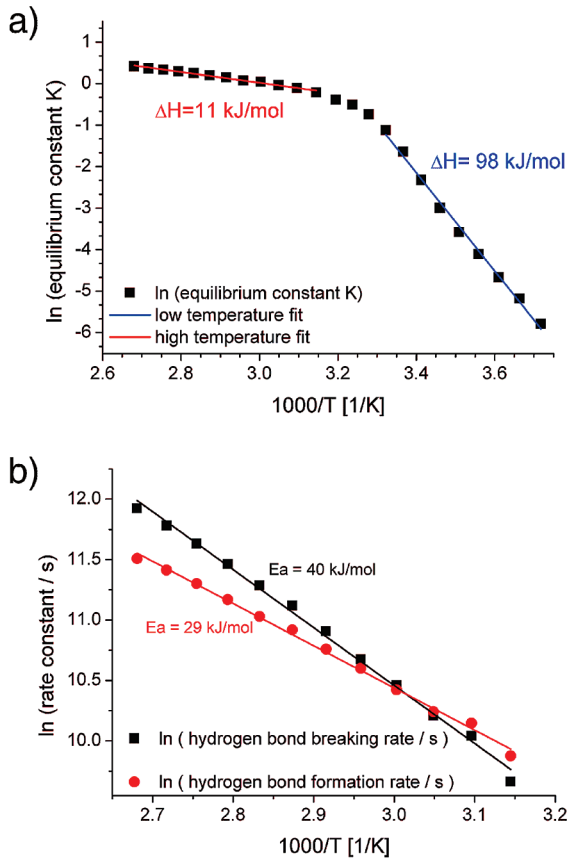

Figure 5. (a) Logarithm of equilibrium constant, K, as a function of inverse temperature. (b) Logarithm of rate constants (k_f, hydrogen bond breaking; k_b, hydrogen bond formation) as a function of inverse temperature with the best fit lines.

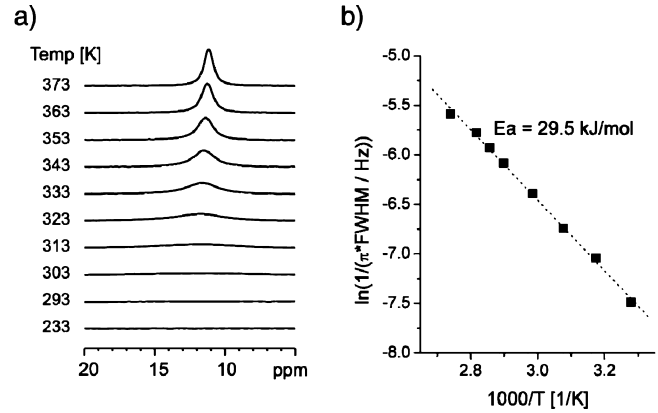

Figure 6. (a) Variable-temperature ^{2}H MAS NMR spectra of deuterated-Tz5Si material recorded at 25 kHz of MAS. (b) Fitting of the ^{2}H line widths against $1000/T$ to get E_a value for acidic ND deuterium mobility. The line width values are extracted between the temperatures of 305 and 365 K. The activation energy for the deuterium motion is additionally given.

of the polymer backbone determines the glass transition. In contrast to the low-temperature process, the high-temperature process has a low reaction enthalpy of 11.0 ± 0.4 kJ/mol, which is favorable for anhydrous proton transport based on a structural diffusion mechanism.[34]

For the proton transport properties, information on the local proton dynamics such as the formation or the breaking of individual hydrogen bonds is much more relevant. Analyzing the line width of the exchange signal in the fast motional limit using eq 4 and combining the results with the determined temperature dependence of the equilibrium constant K, the rate constants for hydrogen bond formation k_b and breaking k_f can be obtained separately. At $T = 330$ K, both rate constants are equal and have a value of ~30 kHz. From an Arrhenius plot of both rate constants k_f and k_b, shown in Figure 5b, the activation energy for hydrogen bond formation $E_{a,b} = 29.0 \pm 0.6$ kJ/mol and the activation energy for hydrogen bond breaking $E_{a,f} = 39.9 \pm 0.9$ kJ/mol can be determined. The given error margins of the activation energies account for statistical errors. In the high-temperature range of our measurements, the average lifetime of an NH−N hydrogen bond, which can be estimated from the inverse of the rate constant k_f, decreases from ~65 μs at $T = 318$ K down to 6.6 μs at $T = 373$ K. Thus, careful analysis of line width and chemical shift of the NH signal in temperature-dependent ^{1}H MAS spectra can provide detailed information on the thermodynamic equilibrium as well as the local dynamics of the NH hydrogen bonding.

Even more detailed information on the molecular dynamics of the NH sites can be expected from ^{2}H NMR experiments, since the orientation dependence of the quadrupolar interaction in the magnetic field is at least 1 order of magnitude higher than the chemical shift difference, leading to the exchange phenomena observed in the ^{1}H MAS spectra.[35−37] Site-selective deuteration of the NH position can be easily achieved by exchanging the acidic NH protons after dissolving the sample in a 3:1 mixture of deuterium oxide and deuterated methanol. After removing the solvent by drying under vacuum, static ^{2}H NMR as well as ^{2}H MAS NMR spectra have been recorded. The static ^{2}H NMR experiments provided very poor signals, caused by the interference of the molecular reorientations of the NH site and the refocusing delay needed for the acquisition of the broad NMR lines.[29] Only at higher temperatures, when the local exchange processes become sufficiently fast, can a broad Lorentzian line shape be observed. The same signal can be recorded under MAS conditions with a much better signal-to-noise ratio due to the periodic refocusing of the signal by MAS. The temperature dependence of the ^{2}H MAS NMR spectra and the Arrhenius plot obtained from the inverse line width of these spectra are given in Figure 6. The activation energy of 29.5 ± 0.8 kJ/mol determined from the ^{2}H NMR experiments matches the activation energy of k_b, keeping in mind that the line width of a NMR signal in the fast motional limit is dominated by the slowest process. Now note that an isotope effect on exchanging ^{1}H by ^{2}H nuclei is not observed. However, isotope contributions of opposite sign are discussed in the literature for mobile hydrogen bonding systems such as water,[38,39] so that sign and magnitude of isotope effects in these systems are difficult to predict and may even vanish.

3.5. Motional Processes of the Triazole Ring versus Hydrogen Bond Dynamics. In addition to the detailed information on the hydrogen bonding of the NH site, variable-temperature ^{1}H MAS NMR measurements also allow for study of the local dynamics of the triazole rings analyzing the temperature dependence of the CH signal. As already described in section 3.3, the CH and the NH signals show a Gaussian line shape at low temperatures, which narrows to a Lorentzian line shape in the temperature range $T = 233−273$ K. This behavior can be explained by a heterogeneous Gaussian distribution of chemical shifts with variance σ due to varying packing arrangements, which start to exchange randomly with increasing temperature. It is difficult to describe this process analytically, but numerical simulations of the line width and the line shape are straightforward. Here, we will not focus on the changes in line shape, which take place in the intermediate

motional regime, where the correlation time of the molecular reorientations τ is comparable to the inverse line width Δ^{-1}. In this particular dynamic regime, however, the observed changes in line shape may strongly depend on the exchange mechanism, e.g., rotational diffusion or random jumps,[36] and thus additional assumptions would be needed to analyze the dynamics. In order to avoid these problems, we focused only on the fast limit, where the static line width is already reduced by more than a factor of 3 compared to the static line width at lowest temperatures.

The full line width Δ at half-height of the observed Lorentzian line shape resulting from randomly exchanging sites within a Gaussian distribution with a variance σ can be used to estimate the exchange rate k:

$$k = \pi(2\sigma)^2\Delta^{-1} = \pi\left(\frac{\Delta_{stat}^{\ 2}}{2\ln 2}\right)\Delta^{-1} \quad \text{for } \frac{\Delta}{\Delta_{stat}} < \frac{1}{3} \qquad (6)$$

Note that the full width at half-height Δ_{stat} of the static Gaussian line shape corresponds to $(8 \ln 2)^{1/2}\sigma$. The approximation in eq 6 corresponds to the result obtained for a symmetric two-site exchange process, when the two resonance lines are separated by a frequency difference of $2(2)^{1/2}\sigma$ (compare eq 4). Moreover, the approximation provides meaningful results only if the line width Δ is at least 3 times smaller than the broadest line width observed at low temperature. In contrast to the two-site exchange case (eq 4), where the exchange rate is overestimated when the fast limit is not fully achieved, the approximation for the Gaussian distribution (eq 6) underestimates the exchange rate k.

At very high exchange rates, the line broadening due to the exchange process becomes comparable to other line-broadening phenomena which have to be taken into account via $T_{2,eff}$ when exchange rates or lifetimes are determined. Since $1/\tau = k + 1/T_{2,eff}$, the exchange rate k can then be determined by

$$k = \frac{\pi}{2\ln 2}\frac{\Delta_{stat}^{\ 2}}{\sqrt{\Delta^2 - (\pi T_{2,eff})^{-2}}} \qquad (7)$$

Here, we estimated $T_{2,eff}$ by the limiting line width of the corresponding signal at the highest temperatures. Using eq 7, the CH line width data given in Figure 4c can be analyzed and the Arrhenius plot given in Figure 7 is obtained. Similar to the analysis of the equilibrium constants K, two different processes with different activation energies are observed. The transition from the low-temperature process to the high-temperature process happens around $T = 313$ K, thus in the same temperature range where the transition between the two processes has been observed in the plot of the equilibrium constants K given in Figure 5a. The activation energy for the high-temperature process is 30.7 kJ/mol, which is similar to the activation energy of hydrogen bond formation (29.0 kJ/mol) but lower than that of the hydrogen bond breaking (40 kJ/mol) in the same temperature range. Therefore, the molecular motions of the triazole ring become more and more effective to break the NH−N hydrogen bond as the temperature increases. However, even at the highest temperature accessible to our MAS probes ($T = 383$ K), the triazole ring experiences on average four to five fluctuations before the NH hydrogen bond breaks and a new hydrogen bond is formed. In the low-temperature regime, an activation energy of 58.3 kJ/mol for the triazole reorientations is obtained from the Arrhenius plot. This activation energy is almost twice that of the high-temperature phase, indicating that there is only limited cooperativity in the ring dynamics in this temperature range where structural reorganization is limited by the glassy polymer matrix. Again, no indication for a typical Vogel−Fulcher or other non-Arrhenius behavior is observed in the range of the glass transition temperature determined by DSC.

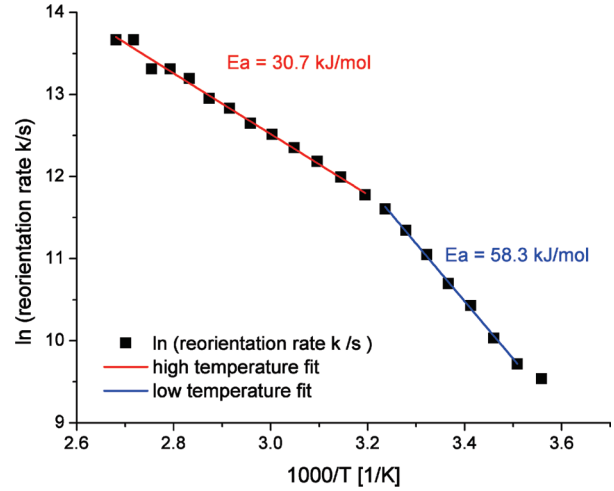

Figure 7. Arrhenius plot of aromatic CH proton reorientation rate. A low-temperature process and a high-temperature process with different activation energies can be distinguished, and the transition temperature between the processes matches that in Figure 4a between the two temperature ranges with different reaction enthalpies.

Concluding the analysis of exchange NMR experiments, we point out that the presented site resolved study of dynamic processes requires sufficient proton chemical shift resolution, which is obtained only for ^{1}H Larmor frequencies higher than 500 MHz and fast MAS at spinning frequencies above 25 kHz. Therefore, it is difficult to extend the experimental range where the ^{1}H MAS NMR spectra are sensitive to the dynamic processes by a variation of the Larmor frequency.

4. Comparison of Microscopic ^{1}H Dynamics and Macroscopic Conductivity

The previous NMR studies monitor local dynamic processes of the triazole rings and their hydrogen bonding to neighboring rings, which are the basic microscopic processes for the anhydrous proton conduction of the material. However, macroscopic transport phenomena such as proton conductivity have additional requirements on mesoscopic length scales. Thus, extrapolation from local processes accessible by spectroscopic NMR methods to macroscopic transport is not straightforward.[7] Nevertheless, we finally want to compare the temperature dependence of the macroscopic proton conductivity determined by impedance spectroscopy with the local dynamics detected by NMR methods.

Assuming that the proton conductivity σ is a thermally activated process, it can be written as

$$\sigma = \sigma_0 e^{-E_a/RT} \qquad (8)$$

Thus, within a given temperature range, an activation energy for the proton conduction can be extracted from the Arrhenius plot of the conductivity shown in Figure 8. The determined activation energies of 56.1 ± 1.1 kJ/mol for the high-temperature regime and 124 ± 3 kJ/mol for the conductivity around the

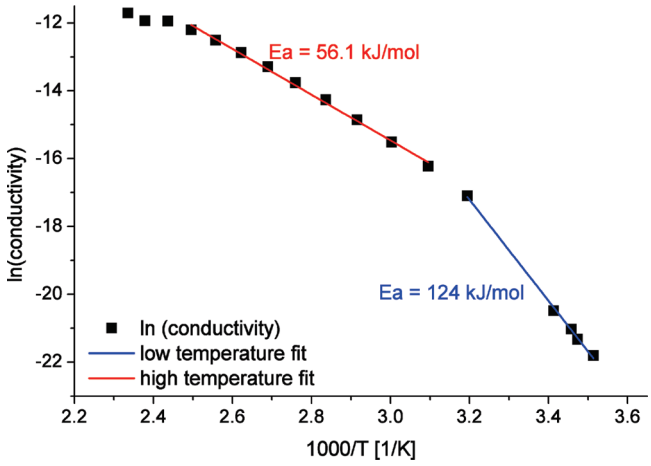

Figure 8. Arrhenius plot of macroscopic conductivity data from impedance spectroscopy. The activation energies of the low- and high-temperature processes have been determined.

glass transition temperature clearly deviate from those determined for the microscopic processes. The transition between the high- and low-temperature regimes, however, is observed at the same temperature range as was found for the ring motion observed via the CH position. This clearly indicates that the molecular motion of the triazole ring is crucial for the proton conductivity of the material. However, proton conduction via the Grotthus mechanism requires the breaking and formation of hydrogen bonds between neighboring triazole rings. Therefore, the activation energies of these processes in the high-temperature regime should be comparable to those from proton conductivity, but the activation energy for the hydrogen bond breaking (40 kJ/mol) corresponds only to 70% of that for the proton conductivity. This difference suggests that indeed other thermally activated processes besides local breaking and formation of hydrogen bonds are essential for proton conduction in Tz5Si.

5. Conclusions

Using solid-state NMR methods, detailed information on the local structure and dynamics of a triazole functional polysiloxane system has been obtained. The presence of strong hydrogen bonding in the solid phase of the material at low temperature was evidenced by the ^{1}H resonance observed at 15.5 ppm. Moreover, the molecular organization at low temperature was probed by 2D ^{1}H DQ NMR spectroscopy, and dimer formation as observed in the case of imidazole-based systems can be safely excluded,[7] due to the missing DQ correlation between hydrogen bonded NH protons in the spectra.

Variable-temperature ^{1}H MAS NMR measurements exhibited remarkable changes in chemical shift, line width, and line shape for the signals of both proton sites at the triazole ring. The temperature dependence of the NH site originates from local fluctuation at temperatures $T < 260$ K and chemical exchange between the NH−N hydrogen bonded and the free state of the protonated heterocyclic site. From the changes in chemical shift a low-temperature process (260 K $< T <$ 300 K) and a high-temperature process ($T > 310$ K) are identified and their free enthalpies are determined to be $\Delta H_{lt} = 98$ kJ/mol and $\Delta H_{ht} =$ 11 kJ/mol, respectively. In the high-temperature regime ($T >$ 320 K), rate constants for hydrogen bond formation and breaking are obtained from the line width of the amine signal. The activation energy for the hydrogen bond breaking $E_{a,f} = 40$ kJ/mol is higher than $E_{a,b} = 29$ kJ/mol for the hydrogen bond formation, indicating increasing population of the free NH state with increasing temperature. Analyzing the substantial line narrowing combined with a change from a Gaussian to a Lorentzian line shape of the CH site in the triazole ring, local fluctuations of the triazole ring are quantified, and the two distinct processes of breaking hydrogen bonds are confirmed. The activation energy of these molecular reorientations $E_{a,tri} =$ 31 kJ/mol in the high-temperature regime is lower than that of the hydrogen bond breaking, indicating that with increasing temperature molecular reorientations of the triazole ring become more efficient at breaking the hydrogen bonding between neighboring rings. However, even at $T = 383$ K, the highest temperature accessible to our probes, the molecular fluctuations are 4−5 times faster than the breaking of the hydrogen bonds.

The observed Arrhenius behavior for limited temperature regimes is characteristic for hidden structural changes in the sample, and it should be noted that the low-temperature process is observed in the same temperature range as the glass transition temperature of Tz5Si observed by DSC. Compared to pure PDMS, this glass transition temperature is increased by ~100 K, indicating the dominating role of the hydrogen bonding between neighboring triazole rings. Moreover, the strong influence of the hydrogen bonding on the structure formation leads to an Arrhenius-like behavior instead of Williams−Landel−Ferry behavior characteristic for the local dynamics of fragile glass formers.

Although the careful analysis of our NMR experiments provides numerous details on the dynamics processes involved in the proton conduction process on the molecular level, a direct comparison of these microscopic results with the macroscopic proton conductivity from impedance spectroscopy is not straightforward. Remarkably, the temperature dependence of the proton conductivity shows as well the two temperature regimes, and the relative ratio between the activation energy in the high-temperature regime and the low-temperature regime matches well, proving that the molecular reorientations of the triazole ring are essential for proton transport. However, all activation energies of the microscopic processes are lower than that of the proton conductivity, indicating that there is an additional energetic barrier controlling the macroscopic proton transport, which is not monitored in the local processes observed by NMR methods.

Acknowledgment. Stimulating discussions with Prof. Andreas Heuer on local molecular dynamics and structural transitions in glass-forming systems are gratefully acknowledged. Partial funding for this work was provided by the NSF-Sponsored Center for Chemical Innovation, and the US Army Green Energy Center at UMass Amherst. A sabbatical fellowship from the Max Planck Gesellschaft to E.B.C. and the hospitality and facilities provided by the Max Planck Institute for Polymer Research in Mainz, Germany, are also gratefully acknowledged.

Supporting Information Available: Figure S1, ^{13}C VT CP-MAS NMR spectra of Tz5Si recorded at 20 kHz MAS with a CP contact time of 2 ms; Figure S2, temperature dependence of ^{1}H DQ-filter signal intensities of the proton sites at the triazole ring; Figure S3, temperature-dependent ^{1}H MAS NMR spectra of poly(vinyltriazole) and Tz5Si.This material is available free of charge via the Internet at http://pubs.acs.org.

References and Notes

(1) Yeo, R. S. *J. Electrochem. Soc.* **1983**, *130*, 533.

(2) Pourcelly, G.; Oikonomou, A.; Gavach, C.; Hurwitz, H. D. *J. Electroanal. Chem.* **1990**, *287*, 43.

(3) Mingos, D. M. P. *Supramolecular Assembly via Hydrogen Bonds*; Springer: Berlin, Germany, 2004.

(4) de Greef, T. F. A.; Meijer, E. W. *Nature* **2008**, *453*, 171–173.

(5) Brown, S. P.; Spiess, H. W. *Chem. Rev.* **2001**, *101*, 4125.

(6) Brown, S. P. *Prog. Nucl. Magn. Reson. Spectrosc.* **2007**, *50*, 199–251.

(7) Goward, G. R.; Schuster, M. F. H.; Sebastiani, D.; Schnell, I.; Spiess, H. W. *J. Phys. Chem. B* **2002**, *106*, 9322.

(8) Lee, Y. J.; Bingol, B.; Murakhtina, T.; Sebastiani, D.; Meyer, W. M.; Wegner, G.; Spiess, H. W. *J. Phys. Chem. B* **2007**, *111*, 9711.

(9) Fischbach, I.; Spiess, H. W.; Saalwachter, K.; Goward, G. R. *J. Phys. Chem. B* **2004**, *108*, 18500–18508.

(10) Hughes, C. E.; Haufe, S.; Angerstein, B.; Kalim, R.; Mahr, U.; Reiche, A.; Baldus, M. *J. Phys. Chem. B* **2004**, *108*, 13626.

(11) Unugur-Celik, S.; Akbey, U.; Graf, R.; Bozkurt, A.; Spiess, H. W. *Phys. Chem. Chem. Phys.* **2008**, *10*, 6058–6066.

(12) Akbey, U.; Graf, R.; Peng, Y. G.; Chu, P. P.; Spiess, H. W. *J. Polym. Sci., Part B: Polym. Phys.* **2009**, *47*, 138–155.

(13) Sezgin, A.; Akbey, U.; Hansen, M. R.; Graf, R.; Bozkurt, A.; Baykal, A. *Polymer* **2008**, *49* (18), 3859–3864.

(14) Unugur-Celik, S.; Akbey, U.; Bozkurt, A.; Graf, R.; Spiess, H. W. *Macromol. Chem. Phys.* **2008**, *209*, 593–603.

(15) Gunday, S. T.; Bozkurt, A.; Meyer, W. M.; Wegner, G. *J. Polym. Sci., Part B: Polym. Phys.* **2006**, *44*, 3315.

(16) Granados-Focil, S.; Woudenberg, R. C.; Yavuzcetin, O.; Tuominen, M. T.; Coughlin, E. B. *Macromolecules* **2007**, *40*, 8708–8713.

(17) Kim, J. D.; Mori, T.; Hayashi, S.; Honma, I. *J. Electrochem. Soc.* **2007**, *154*, A290.

(18) Loren, J. C.; Krasinski, A.; Fokin, V. V.; Sharpless, K. B. *Synlett* **2005**, 2847–2850.

(19) Bielecki, A.; Burum, D. *J. Magn. Reson., Ser. A* **1995**, *116*, 215–220.

(20) Feike, M.; Demco, D. E.; Graf, R.; Gottwald, J.; Hafner, S.; Spiess, H. W. *J. Magn. Reson., Ser. A* **1996**, *122*, 214.

(21) Marion, D.; Ikura, M.; Tschudin, R.; Bax, A. *J. Magn. Reson.* **1989**, *85*, 393–399.

(22) Bennett, A. E.; Rienstra, C. M.; Auger, M.; Lakshmi, K. V.; Griffin, R. G. *J. Chem. Phys.* **1995**, *103*, 6951–6958.

(23) Berglund, B.; Vaughan, R. W. *J. Chem. Phys.* **1980**, *73*, 2037–2043.

(24) Jeffrey, G. A.; Yeon, Y. *Acta Crystallogr., Sect. B: Struct. Sci.* **1986**, *42*, 410–413.

(25) Harris, R. K.; Jackson, P.; Merwin, L. H.; Say, B. J.; Hagele, G. *J. Chem. Soc., Faraday Trans. 1* **1988**, *84* (11), 3649–3672.

(26) Benedict, H.; Limbach, H. H.; Wehlan, M.; Fehlhammer, W. P.; Golubev, N. S.; Janoschek, R. *J. Am. Chem. Soc.* **1998**, *120*, 2939–2950.

(27) Kimura, H.; Shoji, A.; Sugisawa, H.; Deguchi, K.; Naito, A.; Saito, H. *Macromolecules* **2000**, *33*, 6627–6629.

(28) Röhrig, U. F.; Sebastiani, D. *J. Phys. Chem. B* **2008**, *112*, 1267–1274.

(29) Schmidt-Rohr, K.; Spiess, H. W. *Multidimensional Solid-State NMR and Polymers*; Academic Press: London, 1994.

(30) Harris, R. K. *Nuclear Magnetic Resonance Spectroscopy: A Physicochemical View*; Longman Scientific and Technical: Essex, U.K., 1983.

(31) Johnson, C. S. *Adv. Magn. Reson.* **1965**, *1*, 33.

(32) Kühne, R. O.; Schaffhauser, T.; Wokaun, A.; Ernst, R. R. *J. Magn. Reson.* **1979**, *35*, 39.

(33) Angell, C. A. *Science* **1995**, *267*, 1924.

(34) Steininger, H.; Schuster, M.; Kreuer, K. D.; Kaltbeitzel, A.; Bingöl, B.; Meyer, W. H.; Schauff, S.; Brunklaus, G.; Maier, J.; Spiess, H. W. *Phys. Chem. Chem. Phys.* **2007**, *9*, 1764–1773.

(35) Spiess, H. W. *Colloid Polym. Sci.* **1983**, *261*, 193–209.

(36) Lee, Y.-J.; Murakhtina, T.; Sebastiani, D.; Spiess, H. W. *J. Am. Chem. Soc.* **2007**, *129*, 12406–12407.

(37) Thrippleton, M. J.; Cutajar, M.; Wimperis, S. *Chem. Phys. Lett.* **2008**, *452*, 233–238.

(38) Morrone, J. A.; Car, R. *Phys. Rev. Lett.* **2008**, *101*, 017801.

(39) Tachikawa, M.; Shiga, M. *J. Chem. Phys.* **2004**, *121*, 5985–5991.

JP9030909